Journal of
Materials Chemistry B

Accepted Manuscript

This article can be cited before page numbers have been issued, to do this please use: X. Yin, L. Liang, P. Zhao, F. Lan, L. Zhang, S. Ge and J. Yu, *J. Mater. Chem. B*, 2018, DOI: 10.1039/C8TB01552J.

ROYAL SOCIETY OF CHEMISTRY

rsc.li/materials-b

View Article Online
DOI: 10.1039/C8TB01552J

Journal Name

ARTICLE

Double signal amplification based on palladium nanoclusters and nucleic acid cycles on μPAD for dual-model detection of microRNAs

Received 00th January 20xx,
Accepted 00th January 20xx

DOI: 10.1039/x0xx00000x

www.rsc.org/

Xuemei Yin,[a] Linlin Liang,[a, b] Peini Zhao,[a] Feifei Lan,[a] Lina Zhang,[*c] Shenguang Ge[*b] and Jinghua Yu[a]

MicroRNAs (miRNAs) are a sort of significant biomarker, however, it stills a huge challenge to express accurately. Herein, a fluorescent/colorimetric dual-model biosensor based upon quenching effect of graphitic carbon nitride to Palladium nanoclusters (Pd NCs) on the platform of microfluidic paper-based analytical device was built for the detection of miRNAs. On the one hand, the Pd NCs could catalyze chromogenic reaction so that preliminary detection was achieved by the naked eyes. On the other hand, the fluorescent analysis combined with nucleic acid cycle signal amplification was required to get precise result and the detection limit is 3 fM, which was superior to the previous method. What's more, this biosensor could be designed to detect other miRNAs via changing the corresponding aptamer sequences. Therefore, the as-constructed biosensor supplies a versatile platform to conduct point-of-care detection of miRNAs with outstanding performance.

Introduction

MicroRNAs (miRNAs) have only 22 nucleotides in length and belong to endogenous noncoding, single-stranded RNAs.[1] MiRNAs have crucial impacts on cell division, growth, and apoptosis.[2] It has been a fact that some common diseases including cancer,[3] neurological diseases,[4] muscle disorders,[5] and viral infections are closely related with the preternatural expression of some specific miRNAs. For this reason, it is an important biomarker to early clinical diagnosis and an urgent event for quantitative determination of miRNAs.[6] Nevertheless, a series of properties for miRNAs, such as short sequence, low content, easy degradation, and similar sequence among family members, make it an enormous challenge to examine miRNAs accurately and quantitatively.[7]

Single-molecule analysis of microRNA plays an important role in studying molecular biology and genomic diagnostics in various biomolecular systems.[8-10] In particular, signals acquired from single molecule would provide more useful information. Up to mow, many approaches have been developed to express miRNAs. The northern blotting[11] is deemed to exemplary means, but it is necessary to enhance its sensitivity and specificity. Other methods, for instance, microarray technique,[12, 13] quantitative reverse-transcriptase polymerase chain reaction (RT-PCR),[14] isothermally exponential amplification technology,[15] electrochemical method,[16, 17] actualize the detection of miRNAs at a low expression level. However, the methods above usually suffer from slow analysis, false positives, and low sensitivity with large amounts of the sample requirement.[18] Consequently, there is an urgent need to develop an efficient platform, which could not only solve problems mentioned above, but has realized reliable and portable detection of miRNAs. Microfluidic paper-based analytical device (μPAD) proposed by Whitesides[19] has attracted considerable attention.[20, 21] Up to now, colorimetric methodology based on μPAD has been utilized for the qualitative detection of poly-type analytes owing to its briefness, visualization, and cost-effectiveness, but it has relatively low sensitivity.[22] As the complement of colorimetric methodology, fluorescent analysis offers a newfangled method to detect miRNAs which processes high analytical sensitivity, strong selectivity as well as fast response time.[23] Herein, a dual-model analytical μPAD was established based on fluorescent/colorimetric strategy. The superiority of colorimetric screening and fluorescent quantitative analysis was coalescent to reach more reliable diagnostic consequences.

Noble metal nanoclusters (NCs) are a fresh class of materials consisted of dozens of metal atoms, whose diameter distributes at about 2-5 nm.[24] The size equates with Fermi wavelength in which exists the doughty quantum limitation of unbound electrons. Thus metal NCs are in possession of molecular-like properties, including distinctive charging performances and luminescence.[25, 26] Among noble metal NCs, fluorescent palladium NCs (Pd NCs) have attracted

[a] School of Chemistry and Chemical Engineering, University of Jinan, Jinan 250022, P.R. China
[b] Institute for Advanced Interdisciplinary Research, University of Jinan, Jinan 250022, P.R. China. Email: chm_gesg@163.com
[c] Shandong Provincial Key Laboratory of Preparation and Measurement of Building Materials, University of Jinan, Jinan 250022, P.R. China. Email: mse_zhangln@ujn.edu.cn.

View Article Online
DOI: 10.1039/C8TB01552J

considerable interests due to their facile synthesis, peroxidase-like activity, and good photophysical properties.[27, 28] Unique properties have made Pd NCs increasingly applicable to chemical sensing, biological imaging, and cancer therapy.[29, 30] Carbon compounds have been found to be effective in quenching metal NCs. As the most stable allotrope of carbon nitride, graphitic carbon nitride (g-C_3N_4) has been widely applied in the field of photochemical catalysis, colorimetric analysis, and electrochemiluminescent due to fascinating semiconductor characteristic, and thermal and chemical stability.[31, 32] In particular, it has been verified compared with the bulk g-C_3N_4, a few atomic-scale g-C_3N_4 nanosheets (g-C_3N_4 NSs) possess higher water-dispersibility and better biocompatibility.[33, 34] What's more, g-C_3N_4 NSs have more excellent fluorescence quenching property which superior to most of organic dyes.[35]

Inspired by previous study,[36] the work aimed to establish a novel and versatile fluorescent/colorimetric dual-model biosensor on the base of the quenching effect of g-C_3N_4 NSs to Pd NCs and cycle signal amplification on the μPAD for the detection of miRNAs. Compared to preceding miRNAs biosensors, this suggested strategy possessed a number of remarkable virtues. Firstly, Pd NCs served as the fluorescent marker with an excellent peroxidase-like activity, which were superior to most organic fluorescent dyes. Secondly, g-C_3N_4 NSs could be used to an efficient fluorescence quencher which could strongly adsorb DNA through π-π stacking interaction. Thirdly, released miRNAs could be reused in subsequent reaction cycles to realize double signal amplification. Most importantly, the preliminary determination of colorimetric method and the further quantitative detection of fluorescent method were realized simultaneously for ultrasensitive detection of miRNAs based on the dual signal outputs modal. The as-proposed strategy opened a distinctive perspective for designing sensor, and offered a cost-effective, convenient, and disposable μPAD to detect miRNAs quickly and visually, which could be applied in various biological systems and clinical measurements.

Experimental section

Materials and Reagents

All solvents and chemicals related to the cell testing and culture were aseptic after heat sterilization treatment. Hydroxylamine hydrochloride, ascorbic acid (AA, ≥99.0 %) were purchased from Sigma-Aldrich Chemical Co. (Shanghai, China). Shanghai Chemical Reagent Company (Shanghai, China) provided tripolycyanamide, anhydrous ethanol and sodium borohydride ($NaBH_4$). Hydrogen peroxide (H_2O_2), ethylene diamine tetraacetic acid (EDTA), dimethylformamide (DMF) and 3,3',5,5'-tetramethyl benzidine (TMB) were provided by Chemical Reagent Co. (Tianjin, China). Trihydroxymethyl aminomethane (Tris), palladium chloride ($PdCl_2$), sodium dihydrogen phosphate (NaH_2PO_4) and disodium hydrogen phosphate (Na_2HPO_4) were purchased from Aladdin (Shanghai, China). The TE buffer was Tris-EDTA buffer (10 mM, pH 8.0) containing HCl. Ultrapure water was obtained from a Lichun water-purification system (resistivity 18.25 MΩ·cm, Jinan, China). Whatman chromatography paper #1 (58.0 cm × 68.0 cm) (pure cellulose paper) was provided by GE Healthcare Worldwide (Pudong Shanghai, China) and used with further adjustment of size (A4 size). Both the DNA and RNA sequences used in this study were provided by Sangon Biotech Co., Ltd. (Jinan, China), and the sequences of oligonucleotides were listed as follows:

DNA: 5'-AAC TAT ACA ACC TAC TAC CTC A-SH-3'

RNA (let-7a): 3'-UUG AUA UGU UGG AUG AUG GAG U-5'

Apparatus

Ultraviolet-visible (UV-vis) absorption spectra were recorded on a Shimadzu UV-2550 spectrophotometer (Shimadzu, Kyoto, Japan). Scanning electron microscopy (SEM) analyses were obtained from a QUANTA FEG 250 thermal field emission SEM (FEI Co., USA), and energy dispersive X-ray spectroscopy (EDS) information was obtained with an X-MAX50 X-ray energy dispersive spectrometer (Oxford Co., UK), operated at 15 kV. Transmission electron microscopy (TEM) investigations were performed using JEOL JEM-1400 microscope (JEOL, Japan). High resolution transmission electron microscopy (HRTEM) investigation was obtained from JEOL JEM-2100F microscope (JEOL, Japan). Infrared spectroscopy were obtained on a Fourier transform infrared (FT-IR) Spectrum RX (PerkinElmer Spectoment). The fluorescence spectra were obtained on a LS-55 spectrofluorometer (P.E. USA). X-ray diffraction (XRD) patterns were collected on a Pa D8 advance diffractometer system equipped with Cu Ka radiation (Bruker Co., Germany).

Synthesis of g-C_3N_4 NSs

The g-C_3N_4 NSs were prepared based on the previously suggested literature with minor modification.[37, 38] In the first place, the bulk g-C_3N_4 was synthesized in a porcelain crucible with a cover by heating tripolycyanamide at 600 ^{o}C for 2 h under ventilation state with a ramp rate about 3 ^{o}C/min for both of the heating and cooling processes. The bulk g-C_3N_4 was received in the yellow color. Though the g-C_3N_4 NSs could be usually produced via chemically oxidizing the bulk g-C_3N_4 with nitric acid,[39] in this present study, liquid exfoliating was employed for getting water-dispersible g-C_3N_4 NSs. In brief, 100 mg bulk g-C_3N_4 was grinded well into superfine powder and decentralized in 100 mL ultrapure water. Then it was prepared by ultrasound for 18 h. The suspension coming into being initially was centrifuged at 8000 rmp to eliminate the remainder unexfoliated g-C_3N_4. Collect and concentrate supernatant at 60 ^{o}C under vacuum condition to obtain milk-like suspension in a concentration of around 2 g/L.[40] Beyond that, the precipitate was dried into powder for further study.

Synthesis of DNA-Pd NCs

The Pd NCs were composed following the prevenient work with petty modification.[41, 42] $PdCl_2$ solution (150 μL, 0.1 M) and DMF (15 mL) were mixed together, after 5 min, the mix solution was heated under reflux at 150 ^{o}C for 6 h to get the resulting yellow solution. Then, the solution was centrifuged at 8000 rmp to get the Pd NCs. The as-prepared Pd NCs were stored at 4 ^{o}C for further use. Subsequently, 200 μL DNA (10 μM) was introduced into the as-prepared Pd NCs solution (3 mL) to react for 45 min at room temperature for obtaining

View Article Online
DOI: 10.1039/C8TB01552J

DNA-modified Pd NCs (DNA-Pd NCs). The final solution could be stored at 4 °C for about 3 month with few changes.

Design of the μPAD

The μPAD was designed according to the previously reported wax patterning method with slight modification,[43] and the concrete design was illustrated in electronic supplementary information (Fig. S1-S4).

Platinum nanoparticles (Pt NPs) modified μPAD (Pt-μPAD) improved specific surface area, and enlarged surface roughness of μPAD, which was more beneficial to eliminate background fluorescence. The growth of Pt NPs on the μPAD was similar to the previous work,[44] in which H_2PtCl_6 served as metal source and $NaBH_4$ served as reducing agent. In brief, newly synthesized H_2PtCl_6 (20 mM) and $NaBH_4$ (20 mM) were mixed with a certain proportion, then the mixed aqueous solution was dropped to the μPAD surface and dried at ambient temperature for 20 min. Afterwards, ultrapure water was used to wash thoroughly the resulting Pt-μPAD for 3 times, the excess reagents were contacted with a slice bibulous paper at the bottom of the paper working zone, and then drying at room temperature for 30 min. The selection of reductant and optimization of reaction conditions were shown in the electronic supplementary information (Fig. S5, S6).

Construction of the dual-model biosensor

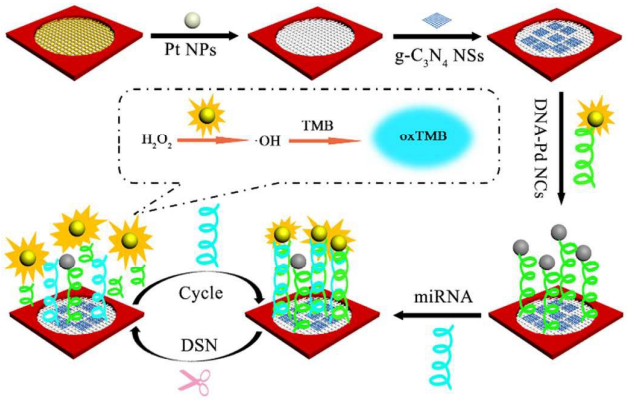

Scheme 1. Schematic representation of the fabrication procedure for the fluorescent/colorimetric dual-model biosensor.

The fabrication of this proposed dual-model biosensor is shown in Scheme 1. Firstly, Pt NPs was grown in the μPAD. Secondly, g-C_3N_4 NSs was applied to Pt-μPAD, followed by the addition of DNA-Pd NCs, and then incubated at ambient temperature for 60 min. Thirdly, 100 μL different concentration of standard let-7a (10^{-3}, 10^{-4}, 10^{-5}, 10^{-6}, 10^{-7}, 10^{-8}, 10^{-9}, 10^{-10}, 10^{-11} μM) was dropped into the corresponding reaction zone in μPAD and incubated at ambient temperature last 30 min to form DNA-RNA heteroduplex. This heteroduplex was disrupted to release free Pd NCs when adding the duplex specific nuclease (DSN). First and foremost, the free Pd NCs were transferred to colorimetric zone of the μPAD. Subsequently, 50 μL 2 % H_2O_2 and 50 μL TMB were also dropped and hatched 20 min at room temperature. In the process, a fast color change occurred and the grey intensity was measured. Consequently, a preliminary test could be come true by naked eyes. If necessary, precise fluorescent detection was implemented. Fluorescence emission spectrum was measured in the range of 400 to 650 nm under excitation at 380 nm.

Results and discussion

Characterization of g-C_3N_4 NSs

In the work, liquid ultrasonic exfoliation was utilized from bulk g-C_3N_4 to get transparent g-C_3N_4 NSs suspension. The SEM image (Fig. 1A) showed the bulk g-C_3N_4 was made up of anomalous folded flakes with the typical few micrometers. Based on SEM and TEM images (Fig. 1B and 1C), it can be clearly found that g-C_3N_4 NSs has typical two-dimensional planar structure with a thickness around 3.5 nm, suggesting the as-synthetized g-C_3N_4 NSs were made up of less than 12 C-N layers.

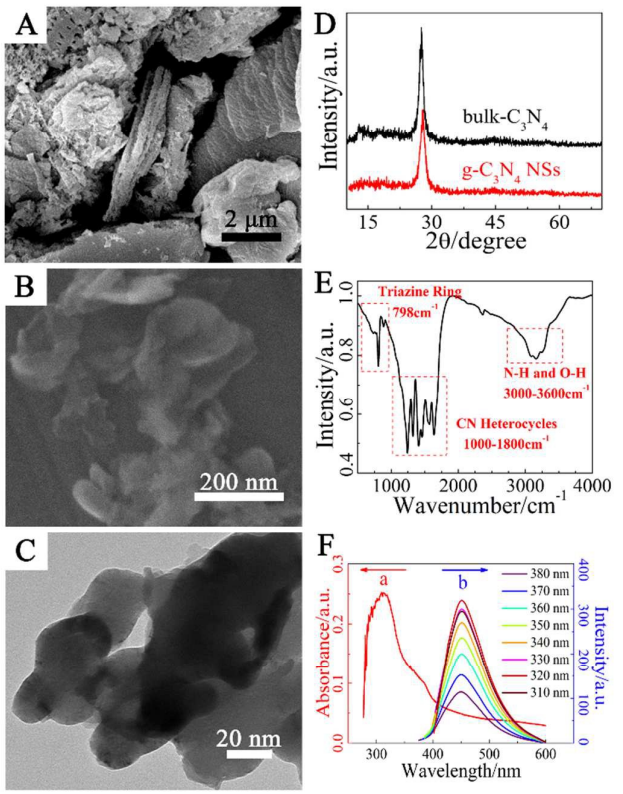

Fig 1. SEM images of (A) bulk g-C_3N_4 and (B) g-C_3N_4 NSs, (C) TEM image of g-C_3N_4 NSs, (D) XRD pattern of bulk g-C_3N_4 and g-C_3N_4 NSs, (E) FT-IR, (F) (a) UV-vis, and (b) Fluorescence spectra of g-C_3N_4 NSs.

The property of synthetized g-C_3N_4 NSs was researched with comprehensive analysis of XRD, FT-IR, fluorescence, and UV-vis. As described in Fig. 1D, the prepared bulk g-C_3N_4 had two diffraction peaks at 13.4 and 27.3°, that 27.3° peak was paralleled with the representative graphitic interlayer stacking peak of g-C_3N_4, and the small peak at 13.4° matched well with the plain packing characteristic in the sheets.[45] However, this g-C_3N_4 NSs only had an individual diffraction peak at 27.7°, in which the interlayer distance slightly reduced from 0.328 nm

View Article Online
DOI: 10.1039/C8TB01552J

(27.3° of the bulk g-C_3N_4) to 0.323 nm (27.7° of the g-C_3N_4 NSs). The result above mainly related to a two-dimensional sheet-like structure of g-C_3N_4 NSs. The XRD pattern manifested bulk g-C_3N_4 was favorably exfoliated to nano-layer structure. For the sake of exploring the functional groups of the g-C_3N_4 NSs, FT-IR spectrum was used to analyze the resulting sample. As can be indicated in Fig. 1E, the g-C_3N_4 NSs showed the vibration of the triazine ring peak at 811 cm^{-1}. The peak from 1000 to 1800 cm^{-1} indicated the stretching pattern of C-N heterocycles, and the peak between 3000 and 3600 cm^{-1} attributed to the stretching vibration of N-H and O-H. The result showed the obtained g-C_3N_4 NSs contain -NH_2 and -OH groups.

In the interest of investigating the optical properties of g-C_3N_4 NSs, UV-vis and fluorescence emission spectrum were studied (Fig. 1F). As illustrated in the UV-vis spectrum (curve a in Fig. 1F), g-C_3N_4 NSs exhibited an intense absorption at 310 nm with a shoulder peak at 366 nm. The g-C_3N_4 NSs also represented an excitation-dependently fluorescent behavior (curve b in Fig. 1F). The emission of g-C_3N_4 NSs changed with the excitation wavelength, since the peaks of emission diverged from 420 to 500 nm as the excitation wavelength changed between 310 and 380 nm. There was the strongest emission in 438 nm when excited at 320 nm. Therefore, wavelength of 320 nm was chosen as the excitation wavelength in the following studies.

Characteristics of Pd NCs

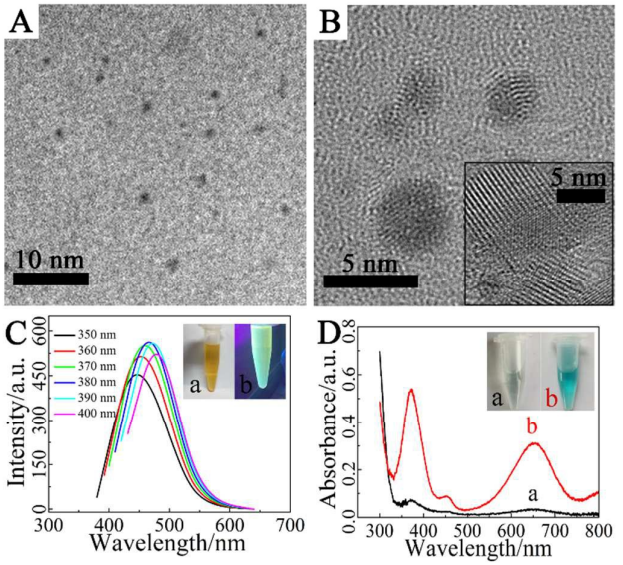

Fig 2. (A) TEM and (B) HRTEM images of Pd NCs, (C) Fluorescence spectrum of Pd NCs. Inset: photographs of Pd NCs before (a) and after (b) excited by an ultraviolet light, (D) UV-vis spectrum of the reaction solution without (a) and with (b) Pd NCs. Inset: photographs of different solutions corresponding to parts a and b.

Pd NCs were a kind of novel fluorescent nanomaterial which was obtained by hydrothermal method.[46] TEM and HRTEM were used firstly to characterize the morphology of Pd NCs. As shown in Fig. 2A, the TEM image demonstrated that Pd NCs were in the form of fine granules with a mean particle diameter of 2-5 nm, indicating good mono-dispersion and homogeneous distribution of Pd NCs. Furthermore, HRTEM image (Fig. 2B) presented the uniform lattice spacing, illustrating the high crystallinity of Pd NCs, which was consistent with the previously reported work.[47] Next, the optical properties of Pd NCs were investigated by the fluorescence spectrum. Fig. 2C showed the fluorescence emission of Pd NCs with different excitation wavelengths. With the excitation wavelength changed between 350 and 400 nm, the fluorescence peak shifted to longer wavelengths with the strongest peak at 460 nm when excited at 380 nm. The Pd NCs presented yellow and transparent solution (inset a in Fig. 2C) and showed strong blue fluorescence excited by an ultraviolet light (inset b in Fig. 2C). TMB, familiar chromogenic substrates, was applied for exploring the peroxidase-like activity of Pd NCs in this study. TMB could be oxidized by Pd NCs to get obvious blue in color with H_2O_2 existed. Fig. 2D showed that owing to the oxidation of TMB, there was the maximum absorbance of the reaction mixture at 650 nm. However, no phenomenon arose when Pd NCs was absent. Insets a and b in Fig. 2D showed the obvious color change before and after the addition of Pd NCs. The results above confirmed that Pd NCs performed an endogenous peroxidase-like property.

Structure characterization of μPAD

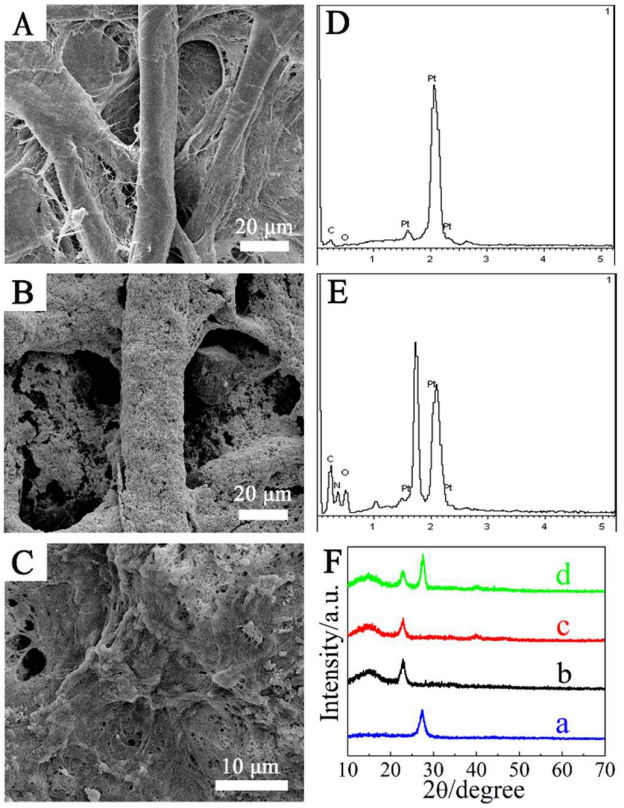

Fig 3. SEM images of (A) μPAD, (B) Pt-μPAD and (C) g-C_3N_4/Pt-μPAD, EDS of (D) Pt-μPAD and (E) g-C_3N_4/Pt-μPAD, (F) XRD pattern of (a) g-C_3N_4 NSs, (b) μPAD, (c) Pt-μPAD and (d) g-C_3N_4/Pt-μPAD.

In order to effectively decrease the background fluorescence of μPAD, the Pt NPs layer was built on the surface

View Article Online
DOI: 10.1039/C8TB01552J

of cellulose fibers to produce an interconnecting Pt-μPAD. The morphologies of the as-prepared bare μPAD, Pt-μPAD and g-C_3N_4/Pt-μPAD were characterized by SEM analysis (Fig. 3). The porous bare μPAD possessed high ratio of surface area to weight (9.5 m^2/g) with smooth microfibers (Fig. 3A). The large-scale Pt NPs were homogeneously grown on the paper-fiber network surface. And the Pt-μPAD still kept fine porous structure, which was beneficial to construct further sensing platform (Fig. 3B). The SEM image of Fig. 3C expressed that the g-C_3N_4 NSs were tightly connected with Pt NPs on the surface of the μPAD. In addition, the EDS analysis were also used to analyze the elemental compositions of Pt-μPAD and g-C_3N_4/Pt-μPAD in the Fig. 3D and 3E. The presence of N and Pt elements indicated that the g-C_3N_4 NSs and Pt NPs were loaded on μPAD, verifying again the successful formation of Pt-μPAD and g-C_3N_4/Pt-μPAD.

Internal structure and material compositions of μPAD, Pt-μPAD and g-C_3N_4/Pt-μPAD were performed by XRD analysis. As indicated in the Fig. 3F, there were two additional representative diffraction reflections at 40 and 46.8° for Pt-μPAD (curve c) compared with the bare μPAD (curve b) which only had two reflections at 14.8 and 24.3°. The reflection of Pt-μPAD was consistent with the Pt standard patterns (JCPD No. 00-004-0802), indicating Pt NPs was deposited successfully on the μPAD. Curve d showed g-C_3N_4/Pt-μPAD consisted of the diffraction peaks of g-C_3N_4 NSs (curve a), μPAD (curve b), and Pt, clearly suggesting the successful preparation of g-C_3N_4/Pt-μPAD.

Possible mechanism for the proposed biosensor

The novel and versatile fluorescent/colorimetric dual-model biosensor was established to detect miRNAs in view of the intensity of the quenching effect of g-C_3N_4 NSs and cycle amplification by DSN on the μPAD. The mechanism of the proposed fluorescent/colorimetric dual-model biosensor was shown in Scheme 1. In this process, the DNA-Pd NCs were adsorbed on the g-C_3N_4 NSs via electrostatic interaction. Therefore, the distance between g-C_3N_4 NSs and DNA-Pd NCs was shortened, meanwhile the fluorescence of Pd NCs was effectively quenched due to photo-induced electron or energy transfer mechanism. Subsequently, the let-7a was added to the miRNA biosensor for forming DNA-RNA heteroduplex. DSN could selectively cleave DNA in double-stranded DNA or in DNA-RNA heteroduplex, then the heteroduplex could be disrupted when DSN was introduced to the platform above. Then, g-C_3N_4 NSs and DNA-Pd NCs were separated from each other, the fluorescence of this system was recovered. More importantly, the released miRNAs could be reused in subsequent reaction cycles simultaneously, realizing the double signal recycle amplification. Subsequently, the free Pd NCs were transferred to the colorimetric region and catalyzed TMB to form the blue product in the existence of H_2O_2.

Fluorescent/colorimetric dual-model analytical detection of let-7a

Under the optimized condition (Fig. S7), let-7a of gradient concentration was quantitatively added to this miRNA biosensor. Colorimetric analysis was performed to detect let-7a visually by dissociative Pd NCs released from target miRNAs. Clearly, the Fig. 4C described that, with the increasing concentration of let-7a, the color changed from light to dark under UV lamp in the existence of TMB and 2 % H_2O_2, which indicated the proposed biosensor particularly attractive for visual detection of let-7a. And the gray intensity also increased gradually as the concentration of let-7a increased. The gray intensity was proportional to the logarithm of the let-7a in the range of 5×10^{-5} to 1 μM, and the linear regression equations was I = 17.24 × lg [let-7a] (μM) + 124.10 (R = 0.993, I = gray intensity). The detection limit of colorimetric analytical method for let-7a was estimated to be about 16 pM (at a signal/noise ratio of 3). What´s more, with the increasing concentration of let-7a, the fluorescence intensity also obviously increased. As demonstrated in the Fig. 4A, weak fluorescence was observed after the addition of 10^{-11} μM let-7a. And with the gradual increase of concentration ranging from 10^{-8} to 10^{-3} μM, obvious fluorescence recovery was found (Fluorescence intensity values are shown in Table S2). There was a good linear relationship between the fluorescence intensity and the logarithmic value of the concentration of let-7a between 10^{-8} and 10^{-3} μM (Fig. 4B). The linear regression equations was ΔI = 122.53 × lg [let-7a] (μM) + 1089.96 (R = 0.997, I = fluorescence intensity). The detection limit was estimated to be 3 fM (at a signal/noise ratio of 3, Table S1 of Electronic supplementary information), which indicates the as-prepared fluorescent/colorimetric dual-model analytical method showed excellent performance, such as wider linear range, lower detection limit, better sensitivity, and higher accuracy, compared with other previously reported methods (Table S3), presenting a promising approach in biosensing and clinical diagnosis.

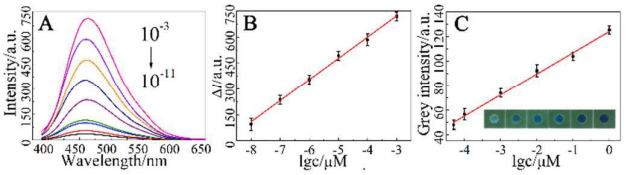

Fig 4. (A) The fluorescence response upon adding the different concentration of let-7a, (B) The calibration curve plotted on a logarithmic scale of fluorescence to let-7a, (C) Colorimetric response of Let-7a and calibration curve plotted on a logarithmic scale.

Specificity, stability, reproducibility of the biosensor

The specificity is a crucial factor for accurate result in the detection of miRNAs. In the work, the same concentration miRNAs of the blank test, let-7a, let-7c, miRNA21, miRNA141 and their mixture was utilized to study the specificity of the biosensor. Fig. 5A showed that the fluorescence intensity of let-7c, miRNA21, miRNA141 was similar to blank test, and far less than that of let-7a. And their mixture did not obviously reveal the change of fluorescence intensity compared to let-7a only. This means the biosensor possesses excellent selectivity towards target miRNAs.

The stability of biosensor is another important factor with regard to its effective use. The biosensor was preserved in the refrigerator with the temperature of 4 ℃ and measured every week for 6 week. As indicated in Fig. 5B, the intensity of the

View Article Online
DOI: 10.1039/C8TB01552J

proposed biosensor has changed little. Even after 6 week, there was about 90 % of fluorescent response remained compared with the initial signal intensity. The data demonstrated the favorable stability of as-constructed biosensor.

The reproducibility was also a crucial requirement for biosensor. The biosensor on the same and different batches was applied to detect miRNAs with same concentration for intra-assay and inter-assay relative standard deviation (RSD). The result indicated that for the same batch biosensor, RSDs were below 4.6 % with colorimetric analysis and 3.4 % with fluorescent analysis at five parallel measurements. For the different batch biosensor, RSDs were less than 5.5 % and 4.1 % for colorimetric and fluorescent detection respectively. The observations above demonstrated that the suggested method had an acceptable reproducibility.

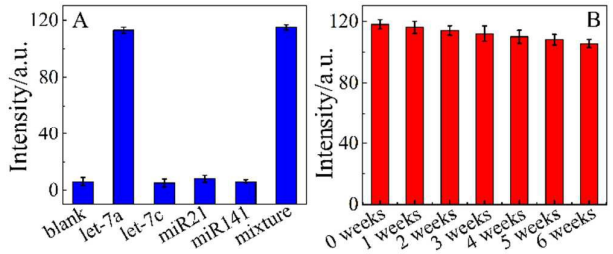

Fig. 5 (A) The specificity of the miRNA biosensor over several miRNAs (the concentration of miRNA was 0.1 pM), (B) The stability of the miRNA biosensor.

Application in practical samples

The potential application of the proposed biosensor to clinical detection was examined through the analysis of several serum samples obtained from Shandong Cancer Hospital. The concrete experimental procedure was summarized as follows: To begin with, the serum samples needed to be diluted appropriately with TE buffer to the miRNAs concentrations in the linear range to obtain the high sensitivity. In the next moment, 100 μL of the diluted serum samples were spiked respectively with 100 μL of standard let-7a miRNAs containing different concentrations (The concentration of standard let-7a miRNAs is proportional). After that, 50 μL of different serum samples were dropped on the prepared biosensor to form DNA-RNA heteroduplex. 30 min later, thorough wash was carried out with PBS solution in the corresponding area to remove unbonded miRNAs and other materials in serums sample. Afterwards, adding the DSN and transferring the free Pd NCs to detection zone of the μPAD, fluorescence emission spectrum was measured under excitation at 380 nm. The quantitation of let-7a in the serums sample was estimated by applying the standard addition method. Finally, the feasibility of the suggested method was obtained by comparing the recovery rate with the standard method. As displayed in Table S4, the recovery values varied in the range of 91.00 to 110.0 %, which was consistent well with traditional RT-PCR (94.00 to 105.0 %). The result above demonstrated the as-proposed biosensor could be potentially applied in real biological samples.

Conclusions

The fluorescence/colorimetric dual-model biosensor was successfully constructed by combining the fluorescence quenching effect of g-C_3N_4 NSs to Pd NCs with the peroxidase-like catalytic performance of the Pd NCs on the μPAD for miRNAs detection. This biosensor took advantage of preliminary visual inspection by color change and accurate fluorescence detection. The as-constructed miRNAs biosensor achieved the double signal recycle amplification by DSN. In addition, the Pt-μPAD not only has increased the specific surface areas, but also decreased significantly the background fluorescence of μPAD. The μPAD device exhibited excellent sensitivity, low detection limit, and favorable selectivity, which provided a kind of relatively rapid and accurate method in point-of-care, qualitative, and quantitative test of various DNAs as well as miRNAs. More importantly, this strategy might not only lay the favorable root for the development of highly effective μPAD in the future, but also offers great application potential in daily life and clinical diagnosis.

Conflicts of interest

There are no conflicts to declare.

Acknowledgements

This work was financially supported by the program for Taishan Scholars of Shandong province (ts201712048), and National Natural Science Foundation of China (21475052, 21775055), as well as the Natural Science Foundation of Shandong Province, China (ZR2017ZC0124). Supports from the 111 Project of International Corporation on Advanced Cement-based Materials (No. D17001) is also greatly appreciated.

References

1 D. M. Vitsios, M. P. Davis, S. van Dongen and A. J. Enright, *Nucleic Acids Res.*, 2017, **45**, 1079-1090.
2 J. Lu, H.-H. Shen, Z. Wu, B. Wang, D. Zhao and L. He, *J. Mater. Chem. B*, 2015, **3**, 7653-7657.
3 Y. Wei, W. Zhou, X. Li, Y. Chai, R. Yuan and Y. Xiang, *Biosens. Bioelectron.*, 2016, **77**, 416-420.
4 K. S. Sheinerman and S. R. Umansky, *Front Cell Neurosci*, 2013, **7**, 150.
5 J. F. Chen, T. E. Callis and D. Z. Wang, *J. Cell Sci.*, 2009, **122**, 13-20.
6 M. Muller, L. Jakel, I. B. Bruinsma, J. A. Claassen, H. B. Kuiperij and M. M. Verbeek, *Mol. Neurobiol.*, 2016, **53**, 2894-2899.
7 A. H. Alhasan, D. Y. Kim, W. L. Daniel, E. Watson, J. J. Meeks, C. S. Thaxton and C. A. Mirkin, *Anal. Chem.*, 2012, **84**, 4153-4160.
8 Z. Chen, Y. Peng, Y. Cao, H. Wang, J. R. Zhang, H. Y. Chen and J. J. Zhu, *Nano. Lett.*, 2018, **18**, 3759-3765.

View Article Online
DOI: 10.1039/C8TB01552J

9 Y. Zhang, Z. Shuai, H. Zhou, Z. Luo, B. Liu, Y. Zhang, L. Zhang, S. Chen, J. Chao, L. Weng, Q. Fan, C. Fan, W. Huang and L. Wang, *J. Amer. Chem. Soc.*, 2018, **140**, 3988-3993.
10 J. D. Harvey, P. V. Jena, H. A. Baker, G. H. Zerze, R. M. Williams, T. V. Galassi, D. Roxbury, J. Mittal and D. A. Heller, *Nat. Biomed. Eng.*, 2017, **1**, 697.
11 Y. S. Choi, L. O. Edwards, A. DiBello and A. M. Jose, *Nucleic Acids Res.*, 2017, **45**, e87.
12 F. Sato, S. Tsuchiya, K. Terasawa and G. Tsujimoto, *PLoS. One*, 2009, **4**, e5540.
13 D. M. Rissin, B. Lopez-Longarela, S. Pernagallo, H. Ilyine, A. D. B. Vliegenthart, J. W. Dear, J. J. Diaz-Mochon and D. C. Duffy, *PLoS. One*, 2017, **12**, e0179669.
14 S. M. Taghdisi, N. M. Danesh, M. A. Nameghi, M. Ramezani and K. Abnous, *Food Chem.*, 2016, **203**, 145-149.
15 W. Ma, B. Situ, W. Lv, B. Li, X. Yin, P. Vadgama, L. Zheng and W. Wang, *Biosens. Bioelectron.*, 2016, **80**, 344-351.
16 J. Zhang, L. L. Wang, M. F. Hou, Y. K. Xia, W. H. He, A. Yan, Y. P. Weng, L. P. Zeng and J. H. Chen, *Biosens. Bioelectron.*, 2018, **102**, 33-40.
17 S. Ge, J. Zhao, S. Wang, F. Lan, M. Yan and J. Yu, *Biosen. Bioelectron.*, 2018, **102**, 411-417.
18 A. Chen, S. Ma, Y. Zhuo, Y. Chai and R. Yuan, *Anal. Chem.*, 2016, **88**, 3203-3210.
19 H. Deng, X. Zhou, Q. Liu, B. Li, H. Liu, R. Huang and D. Xing, *ACS Appl. Mater. Interfaces*, 2017, **9**, 41151-41158.
20 Y. Zhang, L. Zhang, K. Cui, S. Ge, X. Cheng, M. Yan, J. Yu and H. Liu, *Adv. Mater.* 2018, DOI: 10.1002/adma201801588.
21 Q. Kong, Y. Wang, L. Zhang, C. Xu and J. Yu, *Biosen. Bioelectron.*, 2018, **110**, 58-64.
22 L. Liang, S. Ge, L. Li, F. Liu and J. Yu, *Anal. Chim. Acta.*, 2015, **862**, 70-76.
23 Y. Yao, W. Guo, J. Zhang, Y. Wu, W. Fu, T. Liu, X. Wu, H. Wang, X. Gong, X. J. Liang and J. Chang, *ACS Appl. Mater. Interfaces*, 2016, **8**, 22963-22970.
24 Y. Lu and W. Chen, *Chem. Soc. Rev.*, 2012, **41**, 3594-3623.
25 X. L. Hu, X. M. Wu, X. Fang, Z. J. Li and G. L. Wang, *Biosens. Bioelectron.*, 2016, **77**, 666-672.
26 H. Wang, C. Zhou, X. Sun, Y. Jian, Q. Kong, K. Cui, S. Ge and J. Yu, *Biosens. Bioelectron.*, 2018, **117**, 651-658.
27 M. Farrag, *Microporous Mesoporous Mater.*, 2018, **257**, 110-117.
28 Z. Li, X. Yang, N. Tsumori, Z. Liu, Y. Himeda, T. Autrey and Q. Xu, *ACS Catal.*, 2017, **7**, 2720-2724.
29 Z. Peng, Z. Li, Y. Q. Liu, S. Yan, J. Tong, D. Wang, Y. Ye and S. Li, *Chem. Commun. (Camb)*, 2017, **53**, 5958-5961.
30 L. Zhang and E. Wang, *Nano Today*, 2014, **9**, 132-157.
31 L. Jiang, X. Yuan, G. Zeng, X. Chen, Z. Wu, J. Liang, J. Zhang, H. Wang and H. Wang, *ACS Sustainable Chem. Eng.*, 2017, **5**, 5831-5841.
32 K. Ding, X. Zhang, P. Yang and X. Cheng, *CrystEngComm.*, 2016, **18**, 8253-8261.
33 F. Cheng, H. Wang and X. Dong, *Chem. Commun. (Camb)*, 2015, **51**, 7176-7179.
34 R. Li, Y. Zhang, W. Tu and Z. Dai, *ACS Appl. Mater. Interfaces*, 2017, **9**, 22289-22297.
35 Q. Wang, W. Wang, J. Lei, N. Xu, F. Gao and H. Ju, *Anal. Chem.*, 2013, **85**, 12182-12188.
36.K. V. Ragavan, L. S. Selvakumar and M. S. Thakur, *Chem. Commun. (Camb)*, 2013, **49**, 5960-5962.
37 J. Tian, Q. Liu, A. M. Asiri, A. O. Al-Youbi and X. Sun, *Anal. Chem.*, 2013, **85**, 5595-5599.
38 X. L. Zhang, C. Zheng, S. S. Guo, J. Li, H. H. Yang and G. Chen, *Anal. Chem.*, 2014, **86**, 3426-3434.
39 L.-S. Lin, Z.-X. Cong, J. Li, K.-M. Ke, S.-S. Guo, H.-H. Yang and G.-N. Chen, *J. Mater. Chem. B*, 2014, **2**, 1031.
40 L. Chen, X. Zeng, P. Si, Y. Chen, Y. Chi, D. H. Kim and G. Chen, *Anal. Chem.*, 2014, **86**, 4188-4195.
41 H. Kawasaki, H. Yamamoto, H. Fujimori, R. Arakawa, Y. Iwasaki and M. Inada, *Langmuir*, 2010, **26**, 5926-5933.
42 J. Yang, C. Tian, L. Wang and H. Fu, *J. Mater. Chem.*, 2011, **21**, 3384.
43 L. Ge, J. Yan, X. Song, M. Yan, S. Ge and J. Yu, *Biomaterials*, 2012, **33**, 1024-1031.
44 L. Li, Y. Zhang, L. Zhang, S. Ge, H. Liu, N. Ren, M. Yan and J. Yu, *Anal. Chem.*, 2016, **88**, 5369-5377.
45 Y. Tang, H. Song, Y. Su and Y. Lv, *Anal. Chem.*, 2013, **85**, 11876-11884.
46 Q. Xi, D. M. Zhou, Y. Y. Kan, J. Ge, Z. K. Wu, R. Q. Yu and J. H. Jiang, *Anal. Chem.*, 2014, **86**, 1361-1365.
47 J. Athilakshmi, S. Ramanathan and D. K. Chand, *Tetrahedron Lett.*, 2008, **49**, 5286-5288.

View Article Online
DOI: 10.1039/C8TB01552J

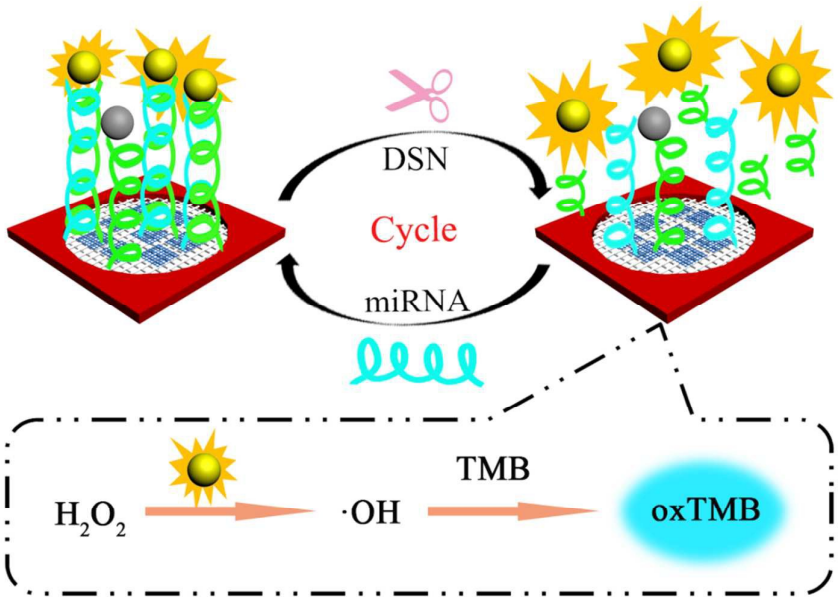

Dual-model signal outputs and double signal amplification on the platform of μPAD for sensitive detection of miRNAs